PHYSICAL REVIEW B **95**, 235432 (2017)

Klein tunneling in the α-T_3 model

E. Illes* and E. J. Nicol
Department of Physics, University of Guelph, Guelph, Ontario N1G 2W1, Canada
and Guelph-Waterloo Physics Institute, University of Guelph, Guelph, Ontario N1G 2W1, Canada
(Received 10 March 2017; revised manuscript received 3 May 2017; published 26 June 2017)

We investigate Klein tunneling for the α-T_3 model, which interpolates between graphene and the dice lattice via parameter α. We study transmission across two types of electrostatic interfaces: sharp potential steps and sharp potential barriers. We find both interfaces to be perfectly transparent for normal incidence for the full range of the parameter α for both interfaces. For other angles of incidence, we find that transmission is enhanced with increasing α. For the dice lattice, we find perfect, all-angle transmission across a potential step for incoming electrons with energy equal to half of the height of the potential step. This is analogous to the "super", all-angle transmission reported for the dice lattice for Klein tunneling across a potential barrier.

DOI: 10.1103/PhysRevB.95.235432

I. INTRODUCTION

According to the Klein paradox [1–4], relativistic particles can readily penetrate large electrostatic potential barriers—a phenomenon that is actually enhanced by increasing the size and width of the potential barrier. In relativistic quantum tunneling, or Klein tunneling, a large potential barrier that is repulsive for incoming particles is attractive for holes, resulting in hole states inside the barrier, and particle states beyond the barrier, connected via particle-hole symmetry. In contrast, nonrelativistic quantum tunneling is exponentially damped with increasing barrier height and the tunneling is facilitated via evanescent waves inside the barrier [5].

Although it was first described by Klein in 1929 [1], experimental realization of relativistic tunneling (akin to Klein tunneling) has only recently become possible [6–9] following the isolation of graphene in 2004 [10]. Graphene, a single-atom thick layer of carbon atoms arranged on a honeycomb lattice (HCL), exhibits low-energy excitations that are well described by the two-dimensional massless Dirac equation, or the Dirac-Weyl equation with pseudospin $S = 1/2$. This has made graphene an ideal playground for directly testing ideas of relativistic physics, including Klein tunneling [6–9] and *Zitterbewegung* [11,12].

Altering the honeycomb lattice of graphene to include an additional atom at the center of the hexagons of the HCL—coupled only to one of the two indistinguishable sites of the bipartite HCL—results in the T_3 or dice lattice [13–16]. Low-energy excitations of the dice lattice are described by the Dirac-Weyl equation with pseudospin $S = 1$.

The α-T_3 model interpolates between the honeycomb lattice of graphene and the dice lattice by allowing the coupling strength between the HCL and the central site to vary from 0 to 1 with parameter α. The lattice for the model is shown in Fig. 1, along with the limiting cases of the HCL ($\alpha = 0$) and the dice lattice ($\alpha = 1$). The α-T_3 model was originally introduced for cold atoms confined to an optical lattice to highlight a dia- to paramagnetic transition in the orbital susceptibility [17] and has been extended to include additional terms or variations [18]. Likewise, a model for three-dimensional (3D) $Hg_{1-x}Cd_xTe$ has been shown to map onto the α-T_3 model in the 2D limit for an intermediate value of the parameter α [19]. Magnetotransport properties [20–22], the Hofstadter butterfly [20], and the effects of the variable Berry phase [23] of the α-T_3 model have been detailed in the literature.

Klein tunneling has been investigated for both of the two limiting cases of the α-T_3 model, i.e., graphene ($\alpha = 0$) and the dice ($\alpha = 1$) lattice. The chiral nature of graphene results in highly anisotropic transmission across barriers for both single and bilayer graphene [24–26]. For a pedagogical review of Klein tunneling across both sharp and smooth barriers in graphene, see Ref. [26]. For the dice lattice, all-angle or "super" transmission across electrostatic barriers has been described for particular values of the incident electron energy [27,28]. The robustness of these results for smoothed potentials was verified via a numerical calculation using a tight-binding model [27]. The confining properties of magnetic barriers have been examined for the dice lattice [27]. Klein tunneling into the flat band across a potential step for generalized pseudospin has been discussed in Ref. [15].

Here, we examine Klein tunneling in the α-T_3 lattice with a focus on the intermediate α regime. We calculate transmission across a sharp potential step and a sharp potential barrier for the lattice. We find perfect transmission for normal incidence for both interfaces for all values of the parameter α. For other angles of incidence, we find a general trend of enhanced transmission with increasing α. Additionally, we investigate transmission across a potential step for the pseudospin $S = 1$ (dice lattice) case. We highlight perfect, all-angle transmission across a potential step for incident electrons with energy equal to half the height of the potential step—akin to the all-angle transmission across potential barriers for the dice lattice [27,28].

The remainder of the paper is laid out as follows. In Sec. II, we introduce the α-T_3 Hamiltonian and develop the required α-dependent matching conditions for connecting wave functions of the α-T_3 lattice across interfaces with sharp changes in potential. In Sec. III, we examine transmission across a sharp potential step for the pseudospin-1 case and the intermediate α regime. In Sec. IV, we investigate transmission across a potential barrier. Conclusions can be found in Sec. V.

*illese@uoguelph.ca

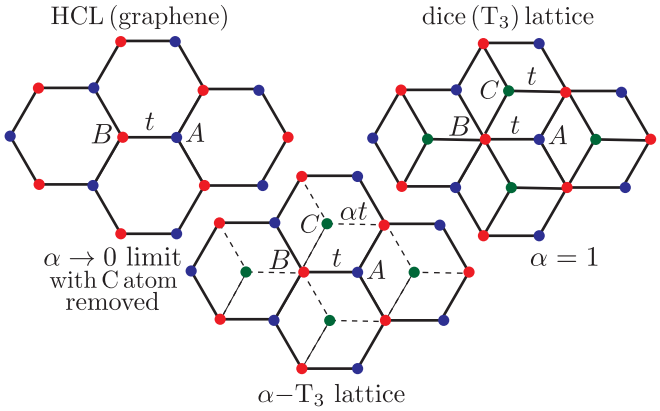

FIG. 1. The α-T_3 lattice is shown in the center with the HCL, its $\alpha \to 0$ limit, on the left and the dice lattice, its $\alpha = 1$ limit, on the right. For the HCL, there are two atoms per unit cell at sites A and B, connected via hopping t. For the other two lattices, there is an additional site C at the center of the hexagons. Site C is connected via hopping parameter t for the dice lattice, and via a variable hopping parameter αt for the α-T_3 model.

II. THEORY AND MODEL

The low-energy Hamiltonian for the α-T_3 model can be written about one K point in the hexagonal Brillouin zone as

$$\hat{H} = \hat{H}_{\rm kin} + V(x)\hat{I}, \tag{1}$$

where $\hat{H}_{\rm kin}$ is the kinetic energy, $V(x)$ is a potential, and I is a 3×3 identity matrix. The kinetic part of the Hamiltonian [17] is given by

$$\hat{H}_{\rm kin} = \begin{pmatrix} 0 & f_k \cos\varphi & 0 \\ f_k^* \cos\varphi & 0 & f_k \sin\varphi \\ 0 & f_k^* \sin\varphi & 0 \end{pmatrix}, \tag{2}$$

where $\alpha = \tan\varphi$ parametrizes the hopping parameter αt, and $f_k = v_F(\xi k_x - i k_y)$, with v_F the Fermi velocity and $\mathbf{k} = (k_x, k_y)$ the wave vector. Here, $\xi = \pm$ is the valley index for the K and K' valleys, respectively, and the Hamiltonian has been rescaled by $\cos\varphi$ for convenience. For $V(x) = 0$, the wave functions are given by

$$|\Psi_s\rangle = \frac{1}{\sqrt{2}} \begin{pmatrix} \cos\varphi\, e^{i\phi} \\ s \\ \sin\varphi\, e^{-i\phi} \end{pmatrix}, \tag{3}$$

with energy $\varepsilon_{k,s} = s v_F |k|$ and $s = \pm$ the band index for the conduction and valence band, respectively. The angle ϕ is defined by $f_k = |f_k| e^{i\phi}$. For the flat band, we have

$$|\Psi_0\rangle = \begin{pmatrix} \sin\varphi\, e^{i\phi} \\ 0 \\ -\cos\varphi\, e^{-i\phi} \end{pmatrix}, \tag{4}$$

with energy $\varepsilon_{k,0} = 0$.

In Secs. III and IV, we will examine transmission across a sharp potential step and a barrier, respectively, by defining a particular potential, $V(x)$ [as in Eq. (1)]. Throughout this work, we will consider potential steps that are smooth on the atomic scale, but sharp on the length scale of the Fermi wavelength [25–27]. Consequently, we will require matching conditions for the wave functions across such interfaces. To determine the relationship between the wave functions on either side of a sharp potential step, we integrate the eigenvalue equation $\hat{H}\Psi = E\Psi$ over a small interval $x = [-\epsilon, \epsilon]$ [15,27] and allow the interval to approach zero. Upon writing our wave function in the general form $\Psi(x) = [\psi_A(x), \psi_B(x), \psi_C(x)]$, we obtain the following matching conditions:

$$\psi_B(-\epsilon) = \psi_B(\epsilon), \tag{5}$$

$$\cos\varphi\, \psi_A(-\epsilon) + \sin\varphi\, \psi_C(-\epsilon) = \cos\varphi\, \psi_A(\epsilon) + \sin\varphi\, \psi_C(\epsilon), \tag{6}$$

for nondiverging potentials, $V(x)$.

Our matching conditions differ from those of the two limiting cases of the α-T_3 model: pseudospin $S = 1/2$ graphene ($\alpha = 0$) and pseudospin $S = 1$ dice lattice ($\alpha = 1$). For graphene, the matching conditions simply require the continuity of each component of the two-component wave function. In contrast, the matching conditions of the dice lattice [27] include a sum of the first and last component of the wave function as in Eq. (6), and can be obtained from Eqs. (5) and (6) by setting $\sin\varphi = \cos\varphi = 1/\sqrt{2}$. For the α-T_3 model, the matching conditions are of the same form as those of the dice lattice ones, but generalized to account for a variable α.

To better understand the matching conditions for the α-T_3 model, we can calculate the probability current using the wave equation $-i\partial_t \psi = \hat{H}\psi$ and the probability conservation equation $\partial_t |\psi|^2 = \nabla \cdot \mathbf{j}$. We find

$$\mathbf{j} = \begin{pmatrix} j_x \\ j_y \end{pmatrix} = v_F \begin{pmatrix} \mathrm{Re}[\psi_B^*(\cos\varphi\psi_A + \sin\varphi\psi_C)] \\ \mathrm{Im}[\psi_B^*(\cos\varphi\psi_A - \sin\varphi\psi_C)] \end{pmatrix}. \tag{7}$$

We see that for the α-T_3 model (as for the dice lattice [27]), the boundary conditions in Eqs. (5) and (6) correspond to the conservation of the probability current traveling perpendicular to the barrier. Note that setting $\cos\varphi = \sin\varphi = 1/\sqrt{2}$ (or, equivalently, $\alpha = 1$) in the above equation recovers the dice lattice probability current, as we would expect.

III. SHARP POTENTIAL STEP

In this section, we will examine the case of transmission across a sharp potential step where the Hamiltonian is given by Eq. (1) with potential $V(x)$ given by

$$V(x) = \begin{cases} 0, & x \leqslant 0 \\ V_0, & 0 < x. \end{cases} \tag{8}$$

We show an example of this setup in Fig. 2, where we have chosen the potential such that the incident electron is in the conduction band and the transmitted electron is in the valence band (i.e., $s = 1$ and $s' = -1$) resulting in an np junction. On both sides of the potential step, the Fermi level is indicated by a blue circle and the blue arrows indicate the direction of the wave vector in each region. Note that in region II, the direction of propagation is opposite to that of the wave vector.

We can write down a wave function for each of the two regions of interest. Region I contains the incident and reflected wave, while region II contains the transmitted wave. The incident electron wave has wave vector $k = (k_x, k_y)$ and propagates at angle ϕ with respect to the k_x axis given by

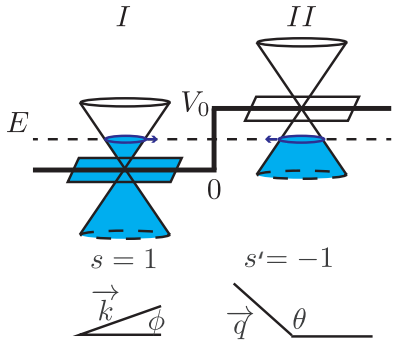

FIG. 2. Schematic depicting a sharp potential step at $x = 0$ with $V_0 > 0$. We have chosen $0 < E < V_0$ for the incoming electron, for which $s = 1$ and $s' = -1$ for the conduction and valence band, respectively. The angles associated with the wave vectors are depicted in the bottom of the figure for each region.

$\tan\phi = k_y/k_x$, while the reflected wave has wave vector $k_r = (-k_x, k_y)$ and propagates at angle ϕ_r given by $\tan\phi_r = k_y/(-k_x)$.

The wave functions in region I can be written

$$|\Psi_I\rangle = \frac{1}{\sqrt{2}}\begin{pmatrix}\cos\varphi\, e^{i\phi}\\ s\\ \sin\varphi\, e^{-i\phi}\end{pmatrix}e^{ik_x x}e^{ik_y y} + \frac{r}{\sqrt{2}}\begin{pmatrix}-\cos\varphi\, e^{-i\phi}\\ s\\ -\sin\varphi\, e^{i\phi}\end{pmatrix}e^{-ik_x x}e^{ik_y y}, \tag{9}$$

for $E \neq 0$, where we have used $\phi_r = \pi - \phi$ for the reflected wave, resulting in $e^{i\phi_r} = -e^{-i\phi}$. In region II, we find the transmitted wave with wave vector q and angle θ given by $\tan\theta = q_y/q_x$ with $q_y = k_y$ from conservation of momentum in the y direction. The wave function in region II is given as

$$|\Psi_{II}\rangle = \frac{t}{\sqrt{2}}\begin{pmatrix}\cos\varphi\, e^{i\theta}\\ s'\\ \sin\varphi\, e^{-i\theta}\end{pmatrix}e^{iq_x x}e^{iq_y y} \tag{10}$$

for $E \neq 0$. We can directly relate the angle θ to the angle of incidence ϕ using conservation of momentum in the y direction to obtain the relationship

$$\sin\theta = \frac{E}{|E - V_0|}\sin\phi, \tag{11}$$

using $k_y = E\sin\phi$ for region I and $k_y = |E - V_0|\sin\theta$ for region II.

Applying the matching conditions in Eqs. (5) and (6) at $x = 0$, we obtain a system of two equations,

$$s + rs = ts', \tag{12}$$

$$A(\phi) - rB(\phi) = tA(\theta), \tag{13}$$

having enforced continuity of $\psi_B(x)$ and continuity of $\cos\varphi\,\psi_A(x) + \sin\varphi\,\psi_C(x)$, respectively. We have defined $A(x) = \cos^2\varphi e^{ix} + \sin^2\varphi e^{-ix}$ and $B(x) = \cos^2\varphi e^{-ix} + \sin^2\varphi e^{ix}$ for convenience. The coefficients r and t can now be calculated as

$$t = \frac{A(\phi) + B(\phi)}{A(\theta) + ss'B(\phi)}, \tag{14}$$

$$r = \frac{A(\phi) - ss'A(\theta)}{B(\phi) + ss'A(\theta)}. \tag{15}$$

Transmission is not, in general, given by $|t|^2$. We must use the conservation of the 1D current in the x direction to obtain

$$|r|^2 + |t|^2\frac{s'\cos\theta}{s\cos\phi} = 1, \tag{16}$$

where the current was calculated using $j = \psi^\dagger S\psi$. For the α-T_3 model, the relevant pseudospin matrices are given by

$$S_x = \begin{pmatrix}0 & \cos\varphi & 0\\ \cos\varphi & 0 & \sin\varphi\\ 0 & \sin\varphi & 0\end{pmatrix}, \tag{17}$$

$$S_y = -i\begin{pmatrix}0 & \cos\varphi & 0\\ -\cos\varphi & 0 & \sin\varphi\\ 0 & -\sin\varphi & 0\end{pmatrix} \tag{18}$$

in the K valley. We can compare Eq. (16) to $R + T = 1$, where R and T are the reflection and transmission probabilities, respectively. This allows us to identify the transmission probability as

$$T = \frac{s'\cos\theta}{s\cos\phi}|t|^2, \tag{19}$$

resulting in

$$T = \frac{4ss'\cos\theta\cos\phi}{2 + 2ss'\cos(\theta + \phi) - \sin^2 2\varphi(s\sin\theta - s'\sin\phi)^2}. \tag{20}$$

We will now proceed to examine the limiting cases and comment on a few special values of the incoming energy E and angle of incidence ϕ.

For normal incidence, Eq. (20) simplifies to $T(\phi = 0) = 1$ for all values of α. This complete transmission is a consequence of the absence of backscattering that results from pseudospin conservation and has already been noted for the two limiting cases of graphene [26] and the dice lattice [27].

For $\alpha = 0$ (or, equivalently, $\cos\varphi = 1$ and $\sin\varphi = 0$), Eq. (20) reduces to the transmission probability of graphene,

$$T_{\text{graphene}} = \frac{2ss'\cos\theta\cos\phi}{1 + ss'\cos(\theta + \phi)}. \tag{21}$$

See Ref. [26] for a detailed discussion of this case.

For the other limiting case of $\alpha = 1$, i.e., the dice lattice, we have $\sin\varphi = \cos\varphi = 1/\sqrt{2}$ which results in a transmission of

$$T_{\alpha=1} = \frac{8ss'\cos\theta\cos\phi}{2 + 4ss'\cos\theta\cos\phi + \cos 2\theta + \cos 2\phi}. \tag{22}$$

In Fig. 3 we present polar plots of the dice lattice transmission probability for a range of E/V_0 ratios where $0 < E < V_0$. For this range, we have $ss' = -1$ (see Fig. 2). For normal incidence, we observe a transmission of $T(\phi = 0) = 1$, as previously noted. For other angles, we observe an increase in the transmission probability as the ratio of E/V_0 increases from 0 to 0.5 and the range of angles about $\phi = 0$ with nearly

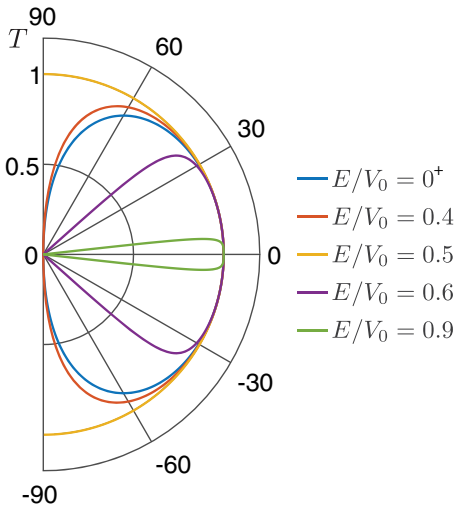

FIG. 3. Transmission across a potential step for the dice lattice ($\alpha = 1$). Transmission curves are plotted as a function of incoming angle ϕ with $0 < E < V_0$ for a range of E/V_0 values.

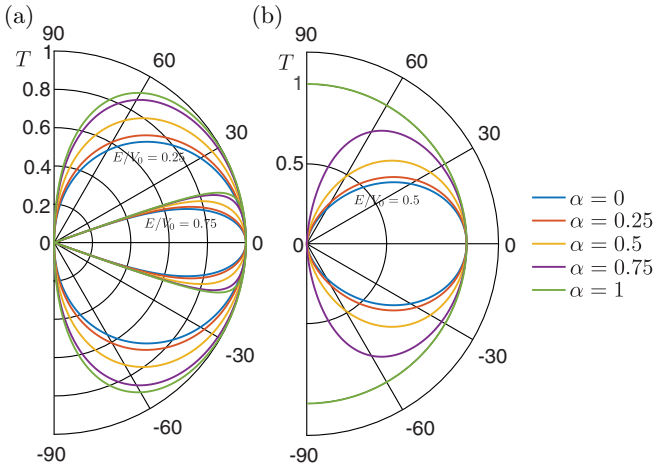

FIG. 4. Transmission across a potential step for a range of α values. Transmission curves are plotted as a function of incoming angle ϕ for (a) $E/V_0 = 0.25$ (outer curves) and $E/V_0 = 0.75$ (inner curves) and (b) $E/V_0 = 0.5$.

perfect transmission grows. This is followed by a decrease in transmission probability as E/V_0 increases from 0.5 and approaches 1 as the range of angles approaching nearly perfect transmission narrows.

For the special case of $E/V_0 = 0.5$, we see a complete transmission of $T(\phi) = 1$ for all incidence angles. This is similar to the "super", all-angle transmission described for the dice lattice for transmission across a potential barrier [27]. In contrast, for graphene, the transmission probability decreases with increasing E for the full range of $0 < E < V_0$, as shown in Ref. [26]. Therefore, the fully transparent potential step, for electrons incident with $E/V_0 = 0.5$ that we noted for the dice lattice ($\alpha = 1$), is absent for graphene.

In Fig. 3, we see that for $E/V_0 > 0.5$, there is a critical angle above which we observe no transmission. This critical angle is given by $\sin\phi_c = \frac{V_0 - E}{E}$ and does not depend on the variable hopping parameter α. Indeed, in Fig. 4(a), we see the same critical angle for the full range of α values for $E/V_0 = 0.75$. For angles of incidence larger than the critical angle, the wave is completely reflected and an evanescent wave with imaginary wave vector q is found in region II. The presence of this critical angle is analogous to the phenomenon of total internal reflection typically discussed in optics.

Examining the special case of $E/V_0 = 0.5$, for general α, we find $\theta = -\phi + \pi$ for the full range of the α-T_3 model. Thus, the step potential with $E/V_0 = 0.5$ can be described as an interface with a negative index of refraction [27,29] of -1, owing to the above relationship between the transmission angle and the angle of incidence. We find the transmission probability governed by

$$T_{(E/V_0=0.5)} = \frac{\cos^2\phi}{1 - \sin^2 2\varphi \sin^2\phi}. \tag{23}$$

Equation (23) is an analytic equation that describes the evolution of the transmission probability from $T = \cos^2\phi$ of graphene to the $T = 1$ of the dice lattice across this interface. In particular, when $\alpha = 1$ and therefore $\sin 2\varphi = 1$, the transmission is uniformly 1, while for all other values of α the transmission probability retains its angular dependence. Therefore, though the step potential exhibits properties akin to an interface with a negative index of refraction [27,29] for the full range of α, there is an angular dependence in the transmission probability for all but the limiting case of the dice lattice—where we observe the super, all-angle transmission. In Fig. 4(b), we plot the transmission in Eq. (23) for a range of α values and observe increasing transmission with increasing α, resulting in a transmission of 1 for the special case of $\alpha = 1$.

Finally, in Fig. 4(a), we show transmission curves for an additional value of the ratio $E/V_0 < 0.5$ and observe a similar enhancement of the transmission probability with increasing α. This trend holds true for the full range of $0 < E/V_0 < 1$.

IV. SHARP POTENTIAL BARRIER

In this section, we will discuss tunneling through a sharp potential barrier of finite width d where the Hamiltonian is given by Eq. (1), with potential $V(x)$ given by

$$V(x) = \begin{cases} 0, & x \leqslant 0 \\ V_0, & 0 < x < d \\ 0, & d \leqslant x, \end{cases} \tag{24}$$

as shown in Fig. 5. We can write the wave functions Ψ_I, Ψ_{II}, Ψ_{III} for the three different regions, namely before the barrier, inside the barrier, and after the barrier, respectively.

In region I, we have the incident and reflected wave, with wave function

$$|\Psi_I\rangle = \frac{1}{\sqrt{2}} \begin{pmatrix} \cos\varphi\, e^{i\phi} \\ s \\ \sin\varphi\, e^{-i\phi} \end{pmatrix} e^{ik_x x} e^{ik_y y} + \frac{r}{\sqrt{2}} \begin{pmatrix} -\cos\varphi\, e^{-i\phi} \\ s \\ -\sin\varphi\, e^{i\phi} \end{pmatrix} e^{-ik_x x} e^{ik_y y}, \tag{25}$$

where r is the amplitude of the reflected wave. Note that we have once again used $\phi_r = \pi - \phi$ for the reflected wave,

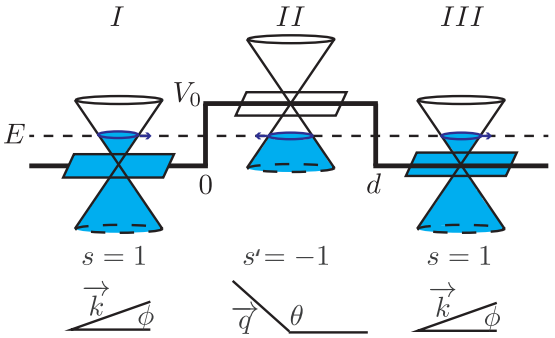

FIG. 5. Schematic for tunneling through a potential barrier that begins at $x = 0$ and has height V_0 and length d. The blue circle represents the Fermi level and the blue arrow indicates the direction of the wave vector. We have chosen $0 < E < V_0$ and $s = 1$ and $s' = -1$ resulting in an *npn* junction. The angles associated with the wave vectors are depicted in the bottom of the figure for each region.

resulting in $e^{i\phi_r} = -e^{-i\phi}$. In region II, we have

$$|\Psi_{II}\rangle = \frac{a}{\sqrt{2}}\begin{pmatrix}\cos\varphi\, e^{i\theta}\\ s'\\ \sin\varphi\, e^{-i\theta}\end{pmatrix}e^{iq_x x}e^{ik_y y} + \frac{b}{\sqrt{2}}\begin{pmatrix}-\cos\varphi\, e^{-i\theta}\\ s'\\ -\sin\varphi\, e^{i\theta}\end{pmatrix}e^{-iq_x x}e^{ik_y y}, \tag{26}$$

where we have two waves traveling in opposite directions with amplitudes a and b. The angle θ is given by $\tan\theta = \frac{q_y}{q_x}$, and conservation of momentum in the $\hat{y}$ direction gives $q_y = k_y$. We can once again relate the angle θ to the incident angle ϕ using Eq. (11).

Finally, in region III, we have the transmitted wave,

$$|\Psi_{III}\rangle = \frac{t}{\sqrt{2}}\begin{pmatrix}\cos\varphi\, e^{i\phi}\\ s\\ \sin\varphi\, e^{-i\phi}\end{pmatrix}e^{ik_x x}e^{ik_y y}, \tag{27}$$

with amplitude t.

Upon applying the boundary conditions found in Eqs. (5) and (6) at the onset of the barrier $x = 0$ and at the end of the barrier $x = d$, we obtain the following expressions for the unknowns a,b,r,t:

$$1 + r = ss'(a + b), \tag{28}$$

$$A(\phi) - rB(\phi) = aA(\theta) - bB(\theta), \tag{29}$$

$$as'e^{iq_x d} + bs'e^{-iq_x d} = tse^{ik_x d}, \tag{30}$$

$$aA(\theta)e^{iq_x d} - bB(\theta)e^{-iq_x d} = tA(\phi)e^{ik_x d}, \tag{31}$$

where we have once again defined $A(x) = \cos^2\varphi e^{ix} + \sin^2\varphi e^{-ix}$ and $B(x) = \cos^2\varphi e^{-ix} + \sin^2\varphi e^{ix}$ for convenience.

In this work, we are primarily concerned with the transmission probability across the barrier, so we only require a solution for t. After some involved algebra, we find

$$t = \frac{4ss'e^{-id(q_x+k_x)}\cos\theta\cos\phi}{e^{-2iq_x d}f_+ - f_-}, \tag{32}$$

where

$$f_\pm = 2 \pm 2ss'\cos(\theta \pm \phi) - \sin^2 2\varphi(s\sin\theta - s'\sin\phi)^2. \tag{33}$$

Finally, we obtain the transmission probability using $T = |t|^2$, after verifying that $T + R = 1$ with $R = |r|^2$. It is given by

$$T = \frac{16\cos^2\theta\cos^2\phi}{f_+^2 + f_-^2 - 2f_+f_-\cos(2q_x d)}. \tag{34}$$

Equation (34) simplifies to the transmission probability across a barrier for graphene [26] and the dice lattice [27] upon substitution of $\alpha = 0$ and $\alpha = 1$, respectively. These cases are discussed in the literature; for example, see Refs. [26] and [27], respectively.

For normal incidence, we find $T(\phi = 0) = 1$ for the full range of α values. This implies complete transmission for an electron incident perpendicular to the barrier, regardless of the size of the barrier or the incoming electron's energy relative to the barrier. This is analogous to what we observed for a sharp potential step in Sec. III.

Similarly to the sharp potential step in Sec. III, we once again find a critical angle ϕ_c for $E/V_0 > 0.5$. Electrons arriving at the interface at an angle exceeding the critical angle can be transmitted through region II in the form of an evanescent wave with imaginary wave vector q.

We now specialize to an intermediate value of the hopping parameter of $\alpha = 0.5$ in order to observe the effect of changing the barrier height relative to the energy of the incident electron in the intermediate regime. In particular, we examine the probability of transmission across a barrier where $V_0 > 0$ and $0 < E < V_0$ (this is the case depicted in Fig. 5). Transmission probabilities for a number of representative E/V_0 ratios and a barrier of length $d = 40V_0$ are shown in Fig. 6.

For small E/V_0, we see a single maximum of $T = 1$ in the transmission probability at $\phi = 0$. As the energy is increased relative to the barrier height, the wave function is able to interfere with itself inside the barrier, akin to being inside a Fabry-Pérot interferometer, resulting in additional resonances marked by $T = 1$ maxima. These resonances occur for $q_x d$ equal to integer multiples of π ($q_x d = n\pi$ with n an integer). Notably, the angle at which the resonances occur is independent of the variable hopping parameter α, which will be further demonstrated in Fig. 7 [see Fig. 7(c)].

Recall that a model for 3D $Hg_{1-x}Cd_xTe$ maps onto the α-T_3 model in the 2D limit for $\alpha = 1/\sqrt{3}$ and α-T_3 behavior has been identified in magneto-optics experiments [19]. The chosen value of $\alpha = 0.5$ in Fig. 6 is close to this α value, perhaps providing some insight for models of $Hg_{1-x}Cd_xTe$ in some limits.

We now examine the dependence of the transmission probability on the variable hopping parameter α. In Fig. 7, we plot the transmission probability for a number of representative E/V_0 ratios for a range of α values, including the special case of $E/V_0 = 0.5$. In general, we see enhanced transmission

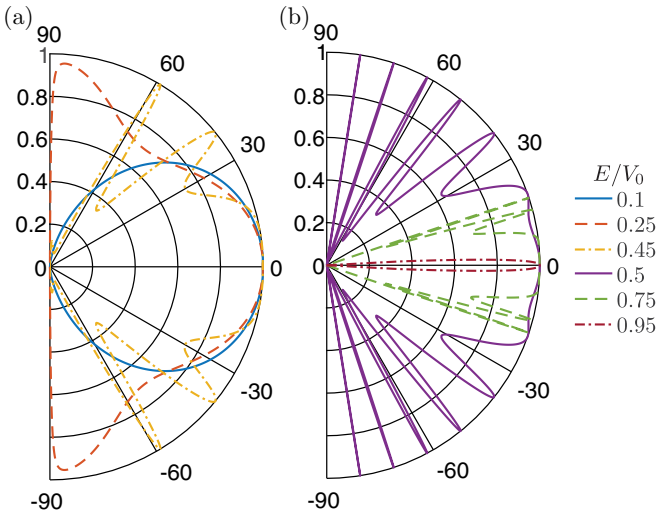

FIG. 6. Polar plot of the transmission probability for $\alpha = 0.5$ for (a) smaller $E/V_0 = 0.1,0.25,0.45$ and (b) larger $E/V_0 = 0.5,0.75,0.95$. The E/V_0 values are shown in the legend. The barrier width is $d = 40V_0$.

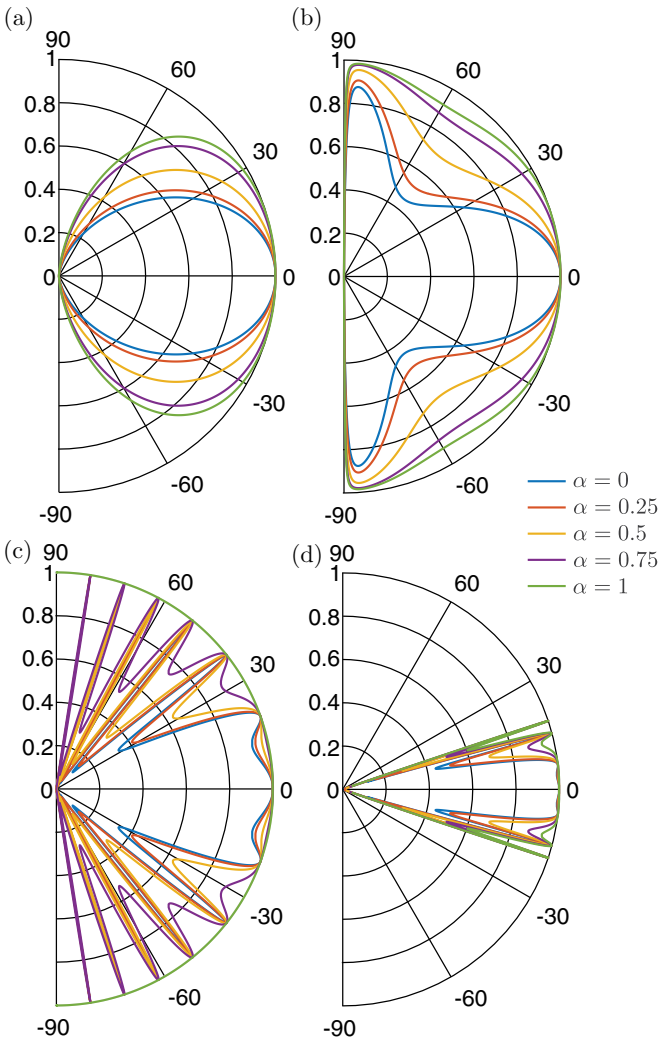

FIG. 7. Polar plot of the transmission probability for a range of α values with (a) $E/V_0 = 0.1$, (b) $E/V_0 = 0.25$, (c) $E/V_0 = 0.5$, and (d) $E/V_0 = 0.75$. The barrier width is $d = 40V_0$.

with increasing α, for all angles where the transmission is not already $T = 1$. As we noted for $\alpha = 0.5$, we again observe Fabry-Pérot resonances for $q_x d$ equal to integer multiples of π. As α is increased from 0 to 1, the sharp resonances of graphene become softer and less pronounced with increasing α. The broadening of the resonance peaks results in increased transmission for angles close to the resonance condition, contributing to the overall trend of enhanced transmission for larger values of α. This is especially dramatic in Fig. 7(c), where $E/V_0 = 0.5$, as the sharp resonances of graphene transform to full transmission of $T(\phi) = 1$ in the $\alpha = 1$ limit. As previously noted in Sec. IV, an np junction with $E/V_0 = 0.5$ acts like a negative index interface with an index of -1 for the full range of α. This holds true for both of the interfaces of the potential barrier, in this case an np and a pn junction. As for transmission across a single potential step, the transmission probability across the barrier retains an angular dependence for all but the limiting case of $\alpha = 1$, where we see the super all-angle transmission.

V. CONCLUSIONS

We have investigated transmission across a sharp potential step and a sharp potential barrier for the α-T_3 lattice.

For electrons incident perpendicular to the interface, we found perfect transmission for the full range of α for both types of interfaces we considered, regardless of the incoming energy of the electron. In general, other angles of incidence enjoyed an enhanced transmission with increasing α, with the exception of those that already had a perfect transmission of $T = 1$.

The potential step was found to be fully transparent for incident electrons with incoming energy equal to half the height of the potential step for the dice lattice, regardless of the angle of incidence. This is analogous to the super transmission across a potential barrier previously reported for the dice lattice [27,28]. For the special case of $E/V_0 = 0.5$, we derived an analytical formula to describe the evolution of the transmission probability from the $T = \cos^2\phi$ of graphene to the $T = 1$ perfect transmission of the dice lattice (as a function of the parameter α).

With regard to transmission across a potential barrier, we found a general trend of enhanced transmission with increasing α. Fabry-Pérot-like resonances were found in the intermediate α regime, as in graphene and the dice lattice. We found the angles at which resonances resulted in perfect transmission of $T = 1$ to be independent of the parameter α. However, the sharp resonances of graphene were broadened with increasing α, but less so for large incidence angles. This manifested as an expanding range of angles with nearly perfect transmission about the resonant angles.

Investigations of tunneling across smooth potential steps in graphene demonstrated that the transmission remains qualitatively unchanged. A reduction of transmission is expected across smooth interfaces, the effects of which are most pronounced for larger angles of incidence [26]. Numerical investigations of tunneling across slightly smoothed potentials for the dice lattice using a tight-binding model have demonstrated the robustness of the super all-angle transmission to scattering between the K and K' valleys for low energies [27].

Thus, in the intermediate regime, we expect our results to also be qualitatively robust to slightly smoothed potentials, and expect a general decrease in transmission with smoothing. Specific calculations with smooth potentials are beyond the scope of this work.

The interpolation between the limiting case of $\alpha = 0$ and $\alpha = 1$ is fairly smooth with regard to transmission across potential steps and barriers. However, this is not necessarily an expected result. There are numerous examples of α-dependent behavior including a dia- to paramagnetic transition in the orbital magnetic susceptibility [17]. Signatures of the intermediate regime can be found in the magneto-optics and the Hofstadter butterfly [20], and the Hall conductivity has additional steps that are only present in the intermediate regime [23]. So, while a smooth interpolation is observed for the case of tunneling, it is not necessarily obvious that this would be the case based on previous work on the model.

We analyzed unconventional transmission properties of the α-T_3 model which interpolates between graphene and the dice lattice. We detailed improved transparency with increasing α for a number of situations. For example, the potential step with $E/V_0 = 0.5$ acted like an interface with a negative index of refraction of -1 for the full range of α and was increasingly transparent with increasing α, culminating in complete transparency for all incident angles for $\alpha = 1$, as noted above. The unconventional transparency experienced by Dirac materials across interfaces such as *np* and *npn* junctions, which act like negative index interfaces, presents possibilities for electron focusing akin to the focusing of light in optics. For example, the idea of a Veselago lens in graphene has been analyzed [29] and is now becoming experimentally feasible [30]. Understanding models of other Dirac-like materials, for example the discussed α-T_3 model, may present additional possibilities for electron focusing and electron optics.

ACKNOWLEDGMENTS

This work has been supported by the Natural Sciences and Engineering Research Council (NSERC) of Canada.

[1] O. Klein, The reflection of electrons at a potential step according to the relativistic dynamics of Dirac, Z. Phys. **53**, 157 (1929).
[2] F. Sauter, Behavior of an electron in a homogeneous electric field according to the relativistic theory of Dirac, Z. Phys. **69**, 742 (1931).
[3] F. Hund, Matter generation in the intuitive and quantized wave pattern of matter, Z. Phys. **117**, 1 (1941).
[4] A. Calogeracos and N. Dombey, History and physics of the Klein paradox, Contemp. Phys. **40**, 313 (1999).
[5] D. J. Griffiths, *Introduction to Quantum Mechanics* (Prentice Hall, Upper Saddle River, NJ, 2004).
[6] N. Stander, B. Huard, and D. Goldhaber-Gordon, Evidence for Klein Tunneling in Graphene *p-n* Junctions, Phys. Rev. Lett. **102**, 026807 (2009).
[7] A. F. Young and P. Kim, Quantum interference and Klein tunneling in graphene heterojunctions, Nat. Phys. **5**, 222 (2009).
[8] R. V. Gorbachev, A. S. Mayorov, A. K. Savchenko, D. W. Horsell, and F. Guinea, Conductance of p-n-p graphene structures with "air-bridge" top gates, Nano Lett. **8**, 1995 (2008).
[9] B. Huard, J. A. Sulpizio, N. Stander, K. Todd, B. Yang, and D. Goldhaber-Gordon, Transport Measurements Across a Tunable Potential Barrier in Graphene, Phys. Rev. Lett. **98**, 236803 (2007).
[10] K. S. Novoselov, A. K. Geim, S. V. Morozov, D. Jiang, Y. Zhang, S. V. Dubonos, I. V. Grigorieva, and A. A. Firsov, Electric field effect in atomically thin carbon films, Science **306**, 666 (2004).
[11] T. M. Rusin and W. Zawadzki, Zitterbewegung of electrons in graphene in a magnetic field, Phys. Rev. B **78**, 125419 (2008).
[12] W. Zawadzki and T. M. Rusin, Zitterbewegung (trembling motion) of electrons in semiconductors: A review, J. Phys.: Condens. Matter **23**, 143201 (2011).
[13] J. Vidal, R. Mosseri, and B. Douçot, Aharonov-Bohm Cages in Two-Dimensional Structures, Phys. Rev. Lett. **81**, 5888 (1998).
[14] J. Vidal, P. Butaud, B. Douçot, and R. Mosseri, Disorder and interactions in Aharonov-Bohm cages, Phys. Rev. B **64**, 155306 (2001).
[15] B. Dóra, J. Kailasvuori, and R. Moessner, Lattice generalization of the Dirac equation to general spin and the role of the flat band, Phys. Rev. B **84**, 195422 (2011).
[16] J. D. Malcolm and E. J. Nicol, Magneto-optics of general pseudospin-*s* two-dimensional Dirac-Weyl fermions, Phys. Rev. B **90**, 035405 (2014).
[17] A. Raoux, M. Morigi, J.-N. Fuchs, F. Piéchon, and G. Montambaux, From Dia- to Paramagnetic Orbital Susceptibility of Massless Fermions, Phys. Rev. Lett. **112**, 026402 (2014).
[18] F. Piéchon, J.-N. Fuchs, A. Raoux, and G. Montambaux, Tunable orbital susceptibility in α-T_3 tight-binding models, J. Phys.: Conf. Ser. **603**, 012001 (2015).
[19] J. D. Malcolm and E. J. Nicol, Magneto-optics of massless kane fermions: Role of the flat band and unusual Berry phase, Phys. Rev. B **92**, 035118 (2015).
[20] E. Illes and E. J. Nicol, Magnetic properties of the α-T_3 model: Magneto-optical conductivity and the Hofstadter butterfly, Phys. Rev. B **94**, 125435 (2016).
[21] Á. D. Kovács, G. Dávid, B. Dóra, and J. Cserti, Frequency-dependent magneto-optical conductivity in the generalized α-T_3 model, Phys. Rev. B **95**, 035414 (2017).
[22] T. Biswas and T. K. Ghosh, Magnetotransport properties of the α-T_3 model, J. Phys.: Condens. Matter **28**, 495302 (2016).
[23] E. Illes, J. P. Carbotte, and E. J. Nicol, Hall quantization and optical conductivity evolution with variable Berry phase in the α-T_3 model, Phys. Rev. B **92**, 245410 (2015).
[24] M. I. Katsnelson, K. S. Novoselov, and A. K. Geim, Chiral tunneling and the Klein paradox in graphene, Nat. Phys. **2**, 620 (2006).
[25] T. Tudorovskiy, K. J. A. Reijnders, and M. I. Katsnelson, Chiral tunneling in single-layer and bilayer graphene, Phys. Scr. **T146**, 014010 (2012).
[26] P. E. Allain and J. N. Fuchs, Klein tunneling in graphene: Optics with massless electrons, Eur. Phys. J. B **83**, 301 (2011).

[27] D. F. Urban, D. Bercioux, M. Wimmer, and W. Häusler, Barrier transmission of Dirac-like pseudospin-one particles, Phys. Rev. B **84**, 115136 (2011).

[28] R. Shen, L. B. Shao, B. Wang, and D. Y. Xing, Single Dirac cone with a flat band touching on line-centered-square optical lattices, Phys. Rev. B **81**, 041410 (2010).

[29] V. V. Cheianov, V. Fal'ko, and B. L. Altshuler, The focusing of electron flow and a Veselago lens in graphene p-n junctions, Science **315**, 1252 (2007).

[30] G.-H. Lee, G.-H. Park, and H.-J. Lee, Observation of negative refraction of dirac fermions in graphene, Nat. Phys. **11**, 925 (2015).